applied sciences

MDPI

Article

Triangular Silver Nanoparticles Synthesis: Investigating Potential Application in Materials and Biosensing

Laura G. Rodriguez Barroso [1], Eduardo Lanzagorta Garcia [1], Marija Mojicevic [1,*], Miriam Huerta [2], Robert Pogue [3], Declan M. Devine [1] and Margaret Brennan-Fournet [1]

[1] PRISM Research Institute, Technological University of the Shannon: Midlands Midwest, Dublin Rd., N37 HD68 Athlone, Ireland; laura.rodriguez@tus.ie (L.G.R.B.); e.lgarcia@research.ait.ie (E.L.G.); declan.devine@tus.ie (D.M.D.); margaret.brennanfournet@tus.ie (M.B.-F.)
[2] Physics Institute, Universidad Autónoma de San Luis Potosí, Av. Parque Chapultepec 1570, San Luis Potosí 78295, Mexico; miriam.huerta@if.uaslp.mx
[3] Campus Asa Norte, Universidade Católica de Brasília, SGAN Módulo B 916 Avenida W5—Asa Norte, Brasilia 70790-160, Brazil; redward@p.ucb.br
* Correspondence: marija.mojicevic@tus.ie

Abstract: Triangular silver nanoplates (TSNPs) exhibit unique optical and antimicrobial properties due to their shape, sharp edges, and vertices. In this study, TSNPs were incorporated into biopolymer blends (bacterial cellulose (BC) with polylactic acid (PLA), polycaprolactone (PCL), and polyhydroxybutyrate (PHB)). Antimicrobial activity of materials was tested against *Escherichia coli* ATCC 95922 and *Staphylococcus aureus* ATCC 25923 (10^6 CFU/mL). After incubation (24 h at 37 °C, 100 rpm), optical density was measured at 630 nm. In order to assess biosensing applications, specifically fibronectin (Fn) behavior, TSNPs were protected with gold (AuTSNP) and analyzed via sucrose sensitivity test and monitored by localized surface plasmon resonance (LSPR). Additionally, AuTSNPs were coated with polyethylene glycol (PEGAuTSNP). Fibronectin functionalization of PEGAuTSNPs and pH-conformation was monitored (FnPEGAuTSNP). Eventually, adequate Fn and anti-Fn antibody concentrations were determined. BC/PHB/TSNPs showed antimicrobial activity against *E. coli* and *S. aureus* with 80 and 95% of growth inhibition, respectively. The sucrose sensitivity test indicated that the $LSPR_{\lambda max}$ of the spectra is directly proportional to the sucrose concentration. $LSPR_{\lambda max}$ of Fn-PEGAuTSNPs at pH 7 and pH 4 were measured at 633 and 643 nm, respectively. A total of 5 µg of Fn was determined to be adequate concentration, while 0.212 mg/mL of anti-Fn antibody indicatied system saturation.

Keywords: nanoparticles; silver; triangular silver nanoplates; biosensing; antimicrobial; biopolymers; fibronectin

Citation: Rodriguez Barroso, L.G.; Lanzagorta Garcia, E.; Mojicevic, M.; Huerta, M.; Pogue, R.; Devine, D.M.; Brennan-Fournet, M. Triangular Silver Nanoparticles Synthesis: Investigating Potential Application in Materials and Biosensing. *Appl. Sci.* **2023**, *13*, 8100. https://doi.org/10.3390/app13148100

Academic Editors: Alexander V. Syuy and Gleb I. Tselikov

Received: 13 June 2023
Revised: 5 July 2023
Accepted: 10 July 2023
Published: 11 July 2023

1. Introduction

The potential applications and synthesis procedures of nanoscale materials were extensively investigated [1–3]. Humans began using metallic nanoparticles (NPs) in ancient times, though were not fully aware of their nature. The earliest examples of NPs in a practical application date back to Mesopotamian and Egyptian cultures when they used metals in the fabrication of glass. Through history, this technique was used and improved, mainly for decorative purposes, allowing glass staining in a variety of colors due to the plasmonic properties of the NPs [4]. While gold nanoparticles were extensively utilized for several decades, the application of silver nanomaterials with similar potential is considerably restricted due to certain seemingly unfavorable characteristics, such as their susceptibility to be quickly oxidized in the presence of halide ions [5].

Silver (Ag) is one of the most attractive metals for the synthesis of nanoparticles because of the wide range of applications derived from its properties. Attributes such as its malleability, conductivity, ductility, resilience, rareness, and antimicrobial properties

made it valuable and convenient for several everyday life purposes through ancient and modern times. The most common applications of Ag include optoelectronics [6], water disinfection [7], diagnostics [8], anti-cancer therapeutics [9], biomedical technologies [10], drug-gene delivery [11], energy science [12], and clinical anti-bacterial purposes, etc. [13,14]. The increasing list of practical uses found for Ag and its NPs present it as highly valuable for current and future technologies and applications. In recent years, there was significant attention focused on enhancing the controlled synthesis methods for triangular silver nanoplates (TSNPs), primarily due to the widespread utilization of these nanoplates in diverse fields, such as surface-enhanced Raman scattering (SERS) detection and the production of antifungal nanocomposites [15]. Due to their shape, sharp edges, and vertices, TSNPs are proven to exhibit distinctive optical and antibacterial properties [16,17]. In comparison to other nanoparticles, TSNPs garnered significant interest due to their ability to tune SPR bands over a wide range by controlling the aspect ratio of the particles [18]. Moreover, the enhanced antimicrobial activity of TSNPs in comparison to spherical nanoparticles is proven to be a consequence of their unique morphology, allowing easier attachment and penetration into the cell membrane and provoking bacterial death [19]. After bacterial membrane damage, the mechanism proposed for antimicrobial action is connected to the formation of reactive oxygen (ROS) and free radical species in high levels inside of the bacteria, inducing their death [20]. Additionally, colloidal stability of NP was proven to play a significant role in antimicrobial action. Controlled growth and ambient media used are critical points for TSNP antimicrobial activity [21].

Silver nanoparticles (AgNP) amalgamated materials are currently used in a range of different applications, including improving electrical and thermal conductivity, water treatment, antimicrobial medical materials, and sensing materials for diagnosis, among others [22]. In the specific case of TSNPs, there are only a limited number of reports of their incorporation into other materials for different applications, and the exploration of the antimicrobial activity of said materials is even more limited. Dispersion of triangular silver nanoprisms in an aqueous acrylamide matrix was reported. The dispersion showed highly tuneable optical properties, and was used as a carrier liquid for a fluorescent dye in the fabrication process of poly(acrylamide) microparticles [23]. Additionally, dispersion of triangular silver microplates in a polyvinylidene fluoride matrix for the improvement of electrical conductivity was reported by [24]. Zhang et al. (2013) fabricated a composite of a TSNPs and chitosan, which significantly enhanced the sensitivity as a surface plasmon resonance (SPR) biosensor [25]. Dithiocarbamaete-stabilized TSNP were used to obtain nanocomposites with polythiophene-derived nanoparticles, in order to obtain a stable system that could be used for applications in catalysis, biosensing, electronics, and optics [26]. The synthesis of solid silver/polyvinylpyrrolidone/polyacrylonitrile nanocomposite films with triangular silver nanoprisms was also reported, taking advantage of their optical absorption spectra to increase the efficiency of photothermal conversion in the polymer matrix, expecting this material to be used in applications such as absorbing materials for solar collectors [27]. Djafari et al. (2019) compared the antimicrobial activity of TSNPs with different polymeric coatings (such as silica, PVP, or mercaptohexadecanoic acid), and found that the surface charge of the selected polymeric coating has an effect on the antimicrobial efficacy of TSNPs towards Gram-positive or Gram-negative strains [28]. Similarly, Vo et al. (2019) studied the feasibility of a gelatin–chitosan coating on the synthesis of TSNPs and evaluated their antimicrobial activity, which was higher than other AgNP morphologies [29]. A chemical method for synthesis of TSNPs and posterior ex situ incorporation into polyvinyl alcohol (PVA) was also reported. Potential applications of this method include dichroic materials and antimicrobial materials, but the antibacterial effects were not evaluated during this study [30]. As the applications for TSNPs can be diverse, their incorporation into polymers for purposes such as improvement of electrical conductivity, thermal conductivity, and biosensing were explored, but there is still a lack of research about their integration into plastics for antimicrobial purposes.

With regard to application in diagnostics, noble metal nanoparticles such as Ag and Au particles exhibit localized surface plasmon resonance (LSPR) in the visible region of the electromagnetic spectrum, making them attractive for sensing applications, as changes can even be detected with the naked eye in some cases, making detection faster, easier, and inexpensive [31]. LSPR is an optical phenomenon that uses the sensitivity of these plasmons' frequency to change the local refractive index at the nanoparticle surface, emerging as a highly sensitive label-free biosensing technique [31]. This presents the LSPR technique as a powerful tool for optical biosensing applications in a range of areas, including biology, biochemistry, and medical sciences, with the potential to be used as portable devices for diagnosis and easy-to-use point-of-care (POC) device platforms [32,33]. In biosensing applications, the nanoparticles' LSPR is used to detect changes in the position of the LSPR bands where the position depends on the nanoparticles' shape, size, uniformity, composition, dielectric environment, local refractive index, and separation distance of NPs [34–37]. To date, several silver nanostructures with high refractive index sensitivities were reported, such as nanorice, nanobipyramids, nanorings, triangular silver nanoplates (TSNPs), and edge gold-coated silver nanoprisms [38]. Among these diverse nanostructures, TSNPs exhibit attractive tunable plasmonic properties due to their sharp corners, and their optical profile displays the strongest and sharpest peaks among all metals [36]. AgNPs are particularly attractive because among all metals, silver possesses the greater scattering cross-section, which means a higher probability of interaction between radiation and the target [39]. Consequently, AgNPs show the most intense plasmonic interaction with incident light, compared to other metallic NPs [40]. Due to their properties, AgNPs are recognized as efficient optical sensors for pesticide residues detection [41]. Moreover, the nanostructure of silver nanoparticles decorated on gold nanoparticles was reported as a sensitive medium for localized surface LSPR biosensing applications [42].

TSNPs are already being used as biosensors in research. For instance, Zhang et al. (2014) used a cytidine 5′-diphospocholine-coated TSNP and AuTSNP (gold-coated TSNP) for detection of C-reactive protein, an inflammatory marker [38]. Brennan-Fournet et al. (2015) successfully detected conformational changes in fibronectin, a protein related to tumor growth and cell survival, using AuTSNPs [43]. Rodriguez Barroso et al. (2023) monitored fibronectin behavior overtime within different complex cellular environments [44]. Vinayagam et al. (2018) built a nanoprobe by conjugating single-strand DNA to the TSNP surface, for specific detection of dengue virus [45]. Cai et al. (2017) proposed a TSNP-AuNP nanoconjugate that allows detection of glucose due to LSPR changes caused by TSNP etching [46]. Fang et al. (2017) also applied TSNP etching color changes in the design of a colorimetric method for the detection of dopamine, which possesses a high affinity to Ag and formed a protective coating against chlorine [47]. A similar approach for the detection of mercury (Hg(II)) was reported, taking advantage of Ag/Hg amalgam formation to protect the TSNP from the effects of chlorine [48]. A slightly contrasting method reported by Furletov et al. (2017), measured the reduction in TSNP color intensity after the addition of Hg(II) alone, attributing such changes to both oxidation by Hg^{+2} ions and amalgam formation [49].

The inconsistent findings regarding the antibacterial and biosensing applications of TSNPs can be attributed to the absence of convenient fabrication methods for producing well-defined anisotropic particles with distinct morphologies, as well as the variations in fabrication approaches employed across different studies. In this study, following up on our previous work, we aimed to prove that our TSNP preparation method can be used for successful incorporation into biopolymer blends (bacterial cellulose (BC) with polylactic acid (PLA), polycaprolactone (PCL), and polyhydroxybutyrate (PHB)), showing high potential for a broad spectrum of applications. Additionally, we investigated potential applications of these nanoplates in biosensing, specifically fibronectin (Fn) conformational behavior within dynamic environments and the detection of this protein with its antibody conjugate, Anti-Fn.

2. Materials and Methods

2.1. Materials

HPLC-grade ultrapure water (34877-2.5L), sodium citrate tribasic (C8532-100G) [TSC], poly(sodium 4-styrenesulfate) (434574-5G) [PSSS], sodium borohydride (213462-25G) [$NaBH_4$], silver nitrate (204390-10G) [$AgNO_3$], L-ascorbic acid (A92902-25G) [AA] and O-[2-(3-mercaptopropionylamino)ethyl]-O′-methylpolyethylene glycol (11124-1G-F) [SH-PEG], gold (III) chloride trihydrate (520918-1G) [$HAuCl_4$], disodium phosphate buffer (30414-500G) ≥99.9–101%, sodium phosphate monobasic monohydrate (71507-1KG), fibronectin bovine plasma [1 mg/mL] (F4759-1G), polyethylene glycol 20000 (8.17018), sucrose (84097-1KG), and anti-Fn antibody (AV41490-100UL) were obtained from Sigma-Aldrich. The FRX pump from Syrris was used for the addition of $AgNO_3$ in the original method and LP-BT100-1F Peristaltic Dispensing Pump with YZII15 pump head and Tygon LMT-55 Tubing (SC0375T) from Drifton (Hvidovre, Denmark) was used for the scaled-up method. Polycaproplactone (PCL) CAPA 6250 was obtained from Perstorp. Ingeo™ polylactic acid biopolymer PLA 4044D was obtained from NatureWorks LLC. PHB (P226) was obtained from Biomer.

2.2. Synthesis of TSNP

The TSNP solution method was adapted from a previously reported seed-mediated approach [50], consisting of a step for seed production and a subsequent step for TSNP growth. Briefly, 5 mL of TSC (2.5 mM), 0.25 mL of PSSS (500 mg/L), and 0.3 mL of NaBH4 (10 mM) were mixed, followed by the addition of 5 mL of $AgNO_3$ (0.5 mM) at a rate of 2 mL/min on constant stirring for the formation of the seed solution. For the TSNP growth, 4 mL of distilled water, 0.075 mL of AA (10 mM), and 0.35 mL of seed solution were mixed, followed by the addition of 3 mL of $AgNO_3$ (0.5 mM) at a rate of 1 mL/min with constant stirring. Finally, 0.5 mL of TSC (25 mM) was added, for a TSNP solution with a final Ag concentration of 21.34 ppm. The chemical reaction occurs as follows [51]:

$$AgNO_3 + NaBH_4 \rightarrow Ag + 1/2H_2 + 1/2B_2H_6 + NaNO_3.$$

Afterwards, in the growth step, the spherical Ag seeds can react with new Ag^+ ions in the presence of ascorbic acid and citrate ions, forming the TSNP. The chemical reaction can be explained as follows [52]:

$$(Spherical\ NPs) + Ag^+ + C_6H_8O_6 \xrightarrow{C_6H_5Na_3O_7} \text{TSNP}.$$

TSC was added at the end of the synthesis to stabilize the nanoplates.

Increased concentration of NPs is desired to aid treatment for the intended TSNP-polymer processing. A reduction of 20% of water for the synthesis was successfully achieved without negatively affecting the results. Different volumes ranging between 0.2 and 0.7 mL were used until 0.35 mL eventually became the standard. Consequently, the adapted method consists of mixing 4 mL of water, 0.075 mL of AA (10 mM), and 0.35 mL of seed solution (25.56 ppm of Ag), followed by the addition of 3 mL of $AgNO_3$ (0.5 mM) at a rate of 1 mL/min. Finally, 0.5 mL of TSC (25 mM) are added when the reaction is finished, resulting in a final Ag concentration of 21.34 ppm and a volume of 8 mL. Noticeably, upon adding $AgNO_3$, the color starts changing from yellow to shades of orange, then shades of red, then purple, and finally takes on a dark blue color, as demonstrated in Figure 1.

Scale-Up of TSNP Production

Unlike the original method where a smaller pump was used, the LP-BT100-1F Peristaltic Dispensing Pump with a YZII15 pump head and Tygon LMT-55 Tubing (SC0375T), provided by Drifton, were used for the addition of $AgNO_3$. The production of TSNP solution was scaled up to a final volume of 300 mL. To achieve this without affecting the synthesis reaction and the final properties of the TSNP, all the volumes and the rate

for addition of $AgNO_3$ were increased proportionally for both the seed solution and the TSNP growth reaction. Thus, to prepare 20 mL of seeds: 8.53 mL of water, 0.95 mL of TSC (25 mM), 0.47 mL of PSSS (500 mg/mL), and 0.57 mL of $NaHB_4$ (10 mM) are mixed, followed by the addition of 9.48 mL of $AgNO_3$ (0.5 mM) at a rate of 3.79 mL/min. After 4 h, the seeds can be used in the second step of the reaction, mixing 150 mL of water, 2.81 mL of AA (10 mM), and 13.12 mL of seed solution (25.56 ppm), followed by the addition of 112.5 mL of $AgNO_3$ (0.5 mM) at the rate of 37.5 mL/min, then 18.75 mL of TSC (25 mM) was added after reaction was finished.

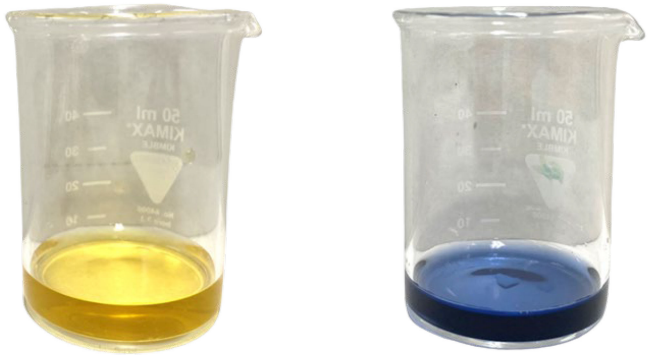

Figure 1. Seed solution (**left**) and TSNP solution (**right**).

A method of water evaporation was used to further increase the concentration of TSNP in the produced solution. A total of 300 mL of the TSNP solution were kept inside the oven at 40 °C for 8 days, until approximately 50% of the water volume was evaporated. UV-Vis spectrum of the solution was recorded before and after heat treatment to monitor the stability of the geometry and optical properties of the TSNP through LSPR. Estimated concentration of the solution after evaporation was 42.64 ppm of atomic silver.

2.3. BC/PHB Blends Preparation

PHB powder, PCL pellets, and PLA pellets were, respectively, dissolved in chloroform to make solutions containing 40 g/L of each polymer. BC production was achieved using *Komagateibacter medelinensis* ID13488 as described in Garcia et al. (2022) [53].

Stripes of 1 × 10 cm of BC were cut and each sample was immersed in 30 mL of polymer solution inside 50 mL Falcon tubes. Tubes containing the samples were incubated overnight at 30 °C and 120 rpm in a horizontal position. After incubation, the films were removed from the solution and left inside the waste fume hood for at least 4 h to allow complete evaporation of the chloroform. The films were immersed in 20 mL of distilled water and autoclaved (121 °C, 15 min) prior to the test of antimicrobial activity.

The obtained BC blends were cut in 1 × 2 cm pieces and each piece was fully immersed into 5 mL of TSNP solution with the highest concentration obtained after the water evaporation method (42.64 µL/mL) and incubated overnight at 30 °C with agitation on a horizontal platform (100 rpm). Afterwards, films were removed from the solution and dried overnight at 60 °C. To estimate the amount of TSNP absorbed from the solution into the BC materials, the UV-VIS spectrum reading of the solution was measured before and after the immersion and incubation, and the difference in the absorbance at the peak of the spectrum, between the initial and final solution, was observed. A calibration curve with dilutions of the TSNP solution was used to obtain an estimation of the resulting concentration based on absorbance.

Scanning electron microscopy (SEM) images were obtained using Mira XMU SEM (Tescan™, Brno, Czech Republic) in back scattered electron mode for surface analysis. The accelerating voltage used was 9 kV. Prior to analysis, tested samples were placed on an aluminum stub and sputtered with a thin layer of gold using the Baltec SCD 005 for 110 at 0.1 mbar vacuum.

Evaluation of Antimicrobial Activity

The antimicrobial activity of all derived materials was evaluated against *E. coli* ATCC 95922 and *S. aureus* ATCC 25923 in Luria-Bertani (LB) broth (10 g/L tryptone, 10 g/L NaCl, and 5 g/L yeast extract, pH 7.2). Overnight cultures of the bacteria were diluted to a concentration of 10^8 CFU/mL to be used as pre-culture. Dried BC films (10 mg of each specimen) were immersed in fresh LB broth and inoculated with 1% (*v*/*v*) from pre-culture, for a final concentration of 10^6 CFU/mL of bacteria. Untreated materials were used as negative control. After incubation for 24 h at 37 °C and 100 rpm, BC films were removed from the cultures and optical density (OD) of the cultivated broth was measured at 630 nm using a Biotek Synergy HT microplate reader (Biotek Instruments GmbH, Bad Friedrichshall, Germany). Growth percentage was calculated using the following equation (Equation (1)).

$$\text{Growth Percentage} = \left(\frac{\text{Absorbance of tested sample}}{\text{Absorbance of positive control}} \right) \times 100 \quad (1)$$

2.4. Evaluation of TSNP Application in Biosensing and Diagnostics

2.4.1. TSNP Gold Coating

Nanoplate protection against etching by chloride ions present in physiological environments was achieved by covering the edges of the nanoplates with gold to keep their plasmonic resonance properties. Gold edge coating of the TSNP was carried out following the method reported by [44], consisting of the use of 20 µL of 0.5 mM $HAuCl_4$ salt and 18.9 µL of 10 mM ascorbic acid per 1 mL of TSNP solution. In this method, there is a reduction in $AuCl_4$ and inhibition of Ag oxidation at the surface of the TSNP, resulting in the deposition of a thin layer of gold in the edges of the TSNP due to galvanic replacement.

2.4.2. AuTSNP Sucrose Sensitivity Test

Assessment of the AuTSNPs performance as nanobiosensors was analyzed through a sensitivity test (sucrose test) adapted from [54] by changing the refractive index of the nanoplates' local environment. A range of AuTSNP volumes were suspended in a 1:1 ratio to different concentrations of sucrose solutions (10%, 20%, 30%, 40%, and 50% (*w*/*v*) in ultrapure water), increasing the refractive index as the sucrose concentration rises. UV-Vis spectrum measurements of each sample were recorded to observe changes in the LSPR spectra.

2.4.3. Polyethylene Glycol Coating of AuTSNP

To secure nanoplate extra protection against the physiological environment for biosensing assays, AuTSNPs were coated with polyethylene glycol (PEG). One of the most researched polymers for coating or stabilizing nanoparticles is polyethylene glycol. Public health agencies granted approval for the use of this biocompatible, neutral, and hydrophilic polymer in biomedical and pharmaceutical applications [37]. The AuTSNP solution was centrifuged at 16,000 rpm at 4 °C for 40 min and the clear supernatant was discarded. The blue pellet of the nanoplates was resuspended with a 0.01% solution of PEG 20,000 at a 1:1 AuTSNP-PEG ratio.

2.4.4. Fibronectin Functionalization of PEGAuTSNP and pH-Conformation Monitoring

AuTSNPs were used to monitor fibronectin (Fn) conformational changes induced under different pH conditions. As described by [43], Fn has a compact, folded conformation under physiological buffer conditions (pH 7.4), but is extended at a more acidic pH. Disodium phosphate buffer (pH 4) and phosphate buffer (pH 7) were prepared to induce Fn conformational transitions. Phosphate buffer NaH_2PO_4, 0.2 M at pH 4.16 was prepared by dissolving 3.12 g of NaH_2PO_4 in 100 mL of NaCl 0.2 M. To prepare the buffer at pH 7.23, 40.5 mL Na_2HPO_4 0.2 M, 9.5 mL NaH_2PO_4 0.2 M, and 50 mL of ultrapure water were mixed. Both buffers were diluted to 0.01 M before use.

PEG-coated AuTSNPs were functionalized with Fn by incubating 25 µg of Fn (1 mg/mL) with 50 µL of PEGAuTSNPs. Upon functionalization, 37.5 µL of Fn-PEGAuTSNPs were incubated with 200 µL of phosphate buffer pH 7.2 and pH 4.1, respectively. UV-Vis measurements were performed to record the protein structural changes.

2.4.5. Determination of Adequate Fn Concentration

To ensure successful coating of the nanoplates: 1 µg, 5 µg, 8 µg, 10 µg, and 15 µg of Fn (antigen Ag) were added to different 1 mL aliquots of PEGAuTSNPs and analyzed in a 96-well plate to observe the minimum volume required to observe a difference in the LSPR spectrum, and 1 µg of anti-Fn antibody (Ab) was added to each of the scanned samples after the first reading and analyzed again to observe shift differences upon antibody–antigen binding.

2.4.6. Determination of Adequate Anti-Fn Antibody Concentration

Varied concentrations of antibody were added to a sample of Fn-PEGAuTSNPs to determine the limit of detection (LOD) of the Ag-Ab system. A total of 5 µg of Fn was incubated with 1 mL of PEGAuTSNP. A sample of 99 µL of Fn-PEGAuTSNPs was placed in a well of a 96-well plate and 1 µg of anti-Fn antibody was added and analyzed in the microplate reader. Subsequently, 2 µg, 4 µg, 6 µg, 8 µg, 10 µg, 12 µg, and 14 µg of anti-Fn antibody were added to the well and readings were performed between each concentration. The experiment was performed in the same well to avoid variations and preserve uniformity.

3. Results

3.1. Synthesis of TSNP

Figure 2 shows the normalized UV-Vis spectrum of the seeds and the TSNP prepared using 200 µL of seeds, and afterwards with the modified method (with 350 µL seeds) for increased concentration. TSC and PSSS were used as stabilizers for the seed production, and both were reported to aid the formation of the nanoplates. It is postulated that citrate ions and PSSS (being a charged polymer), bind to the surface of the face of the particles, promoting growth of the NPs in a triangular plate shape [5,50]. When the TSNP synthesis procedure was modified, the amount of silver in the nanoplate solution increased to 21.962 ppm, which led to a narrower LSPR spectrum of ~115 FWHM showing homogeneity of the TSNP with edge lengths around 20–25 nm [38,50] (Figure 2). The triangular morphology of the TSNP prepared through this method was evaluated using TEM on a previous study performed by our team (Figure 3), where the same synthesis method for the TSNP was used [55].

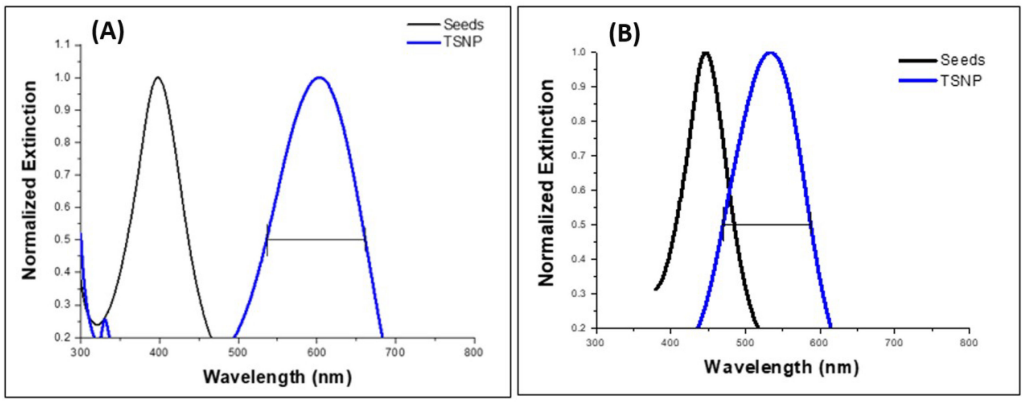

Figure 2. (**A**): UV-Vis spectrum of Ag seeds and TSNPs (200 µL seeds), (**B**): UV-Vis spectrum of Ag seeds and TSNPs prepared with the optimized method (350 µL seeds).

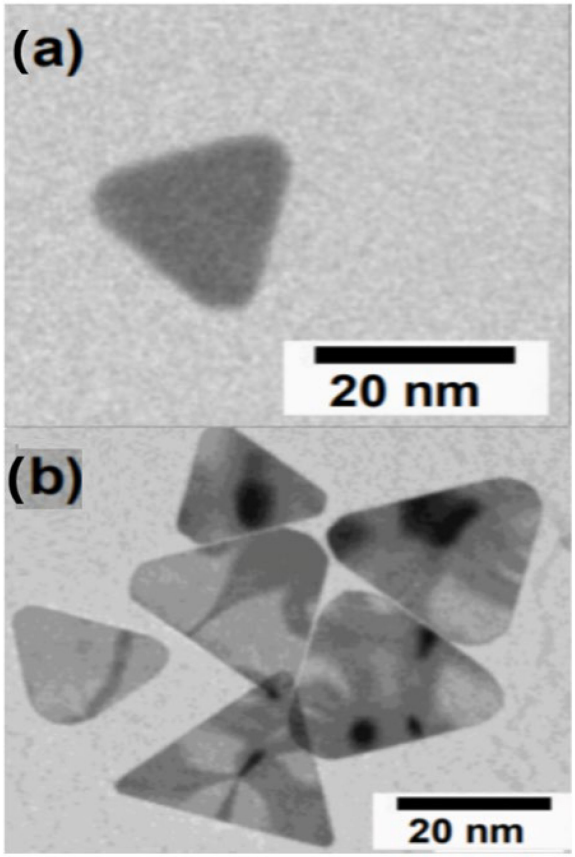

Figure 3. Transmission electron microscopy (TEM) images of (**a**) single TSNP and (**b**) multiple TSNP. Adapted from a previous study [55].

3.2. Scale-Up TSNP Production and Increase in Concentration via Thermal Evaporation

Figure 4 shows the normalized UV-Vis spectrum for the scaled-up TSNP solution. LSPR peak wavelength is 584 and FWHM of 112 nm (635–523 nm). Although there is a small blue shift in the peak and a small reduction in FWHM compared to the results obtained from smaller volumes, these differences are not expected to represent a reduction in antimicrobial activity or in the stability of the nanoparticles, hence, the scale up method is considered functional. Figure 5 shows the resulting UV-Vis spectrum of TSNPs (21.34 ppm) before evaporation, with an LSPR peak wavelength of 621 nm. After incubation, peak wavelength presented a small blue shift to 617 nm and the concentration was estimated to be approximately 43 ppm. FWHM also exhibited a change from 153 nm (707–554 nm) of the original solution to 178 nm (722–544 nm). Considering the prolonged time inside the oven, differences between both spectra were not significant and were not considered an issue, as increasing the concentration is the principal objective of this method.

3.3. Integration of TSNP in Biopolymers for Enhanced Antimicrobial Activity

3.3.1. Preparation of BC Blends with the Addition of TSNP

Following previous examples of integrating TSNPs into polymeric matrices for antimicrobial purposes [53,55], blends of BC with PHB, PLA, and PCL were prepared. After drying the BC/PHB blends, the amount of polymer incorporated into the BC was determined by weighing the dry BC and the films after immersion in the polymer solution. For PHB, approximately 15% of the final weight was accounted for by the incorporated polymer. In the case of PCL, this value was approximately 45%, while for PLA, it was approximately 50%. The BC blends initially showed a milky and white color, but they turned dark blue after immersion in the TSNP solution, corroborating the incorporation of TSNPs into the materials. The amount of TSNPs absorbed by each film was calculated by

measuring the maximum absorbance point on the spectrum of the TSNP solution before and after the immersion and incubation of the BC materials. After contrasting the obtained absorbance values with a calibration curve for the concentration of TSNPs, the amounts absorbed by the materials were estimated as the difference between the initial amount in the solution vs. the final amount after incubation. The average weight of incorporated TSNPs was estimated to be approximately 200 µg for BC/PHB, 153 µg for BC/PCL, and 116 µg for BC/PLA, on each of the 1 × 2 cm pieces, respectively. Figure 6 shows that the BC/PHB samples exhibited the most homogeneous blue coloration throughout the film and they incorporated the largest amount of TSNPs compared to the blends with PLA and PCL. Figure 7 shows the distribution of TSNP clusters on the surface of BC through SEM images.

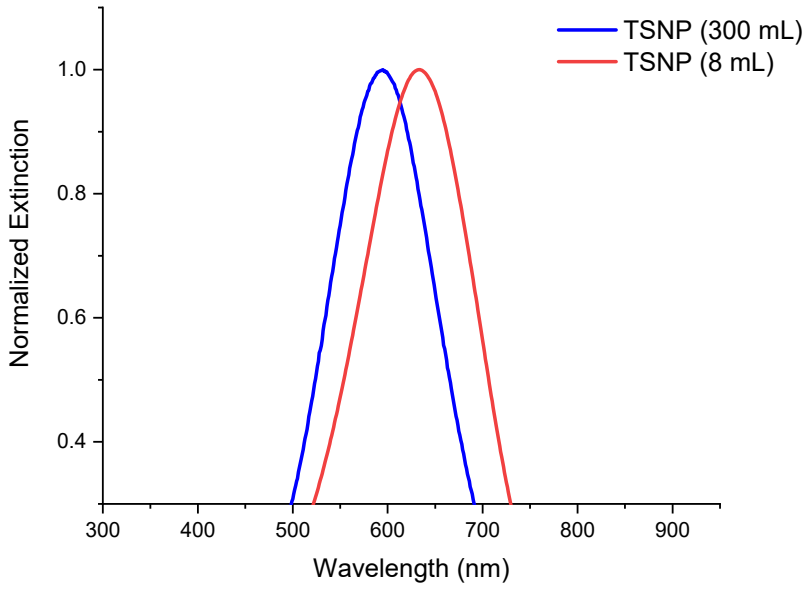

Figure 4. UV-Vis spectrum of scaled-up TSNPs (300 mL) compared to original synthesis method (8 mL).

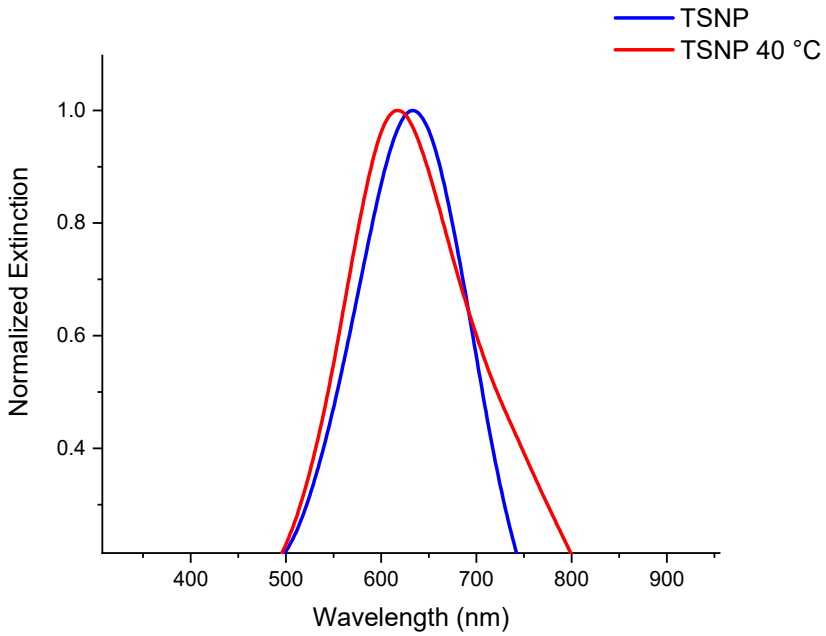

Figure 5. UV-Vis spectra of TSNPs before and after evaporation at 40 °C.

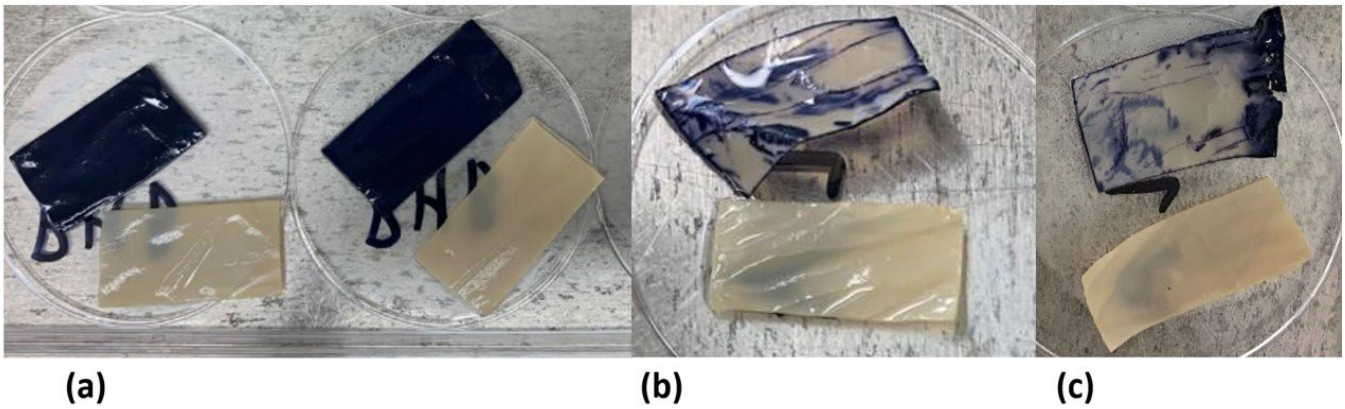

Figure 6. Bare BC blends (white) and BC/TSNP blends (dark blue). (**a**) BC/PHB blends, (**b**) BC/PLA blends, and (**c**) BC/PCL blends.

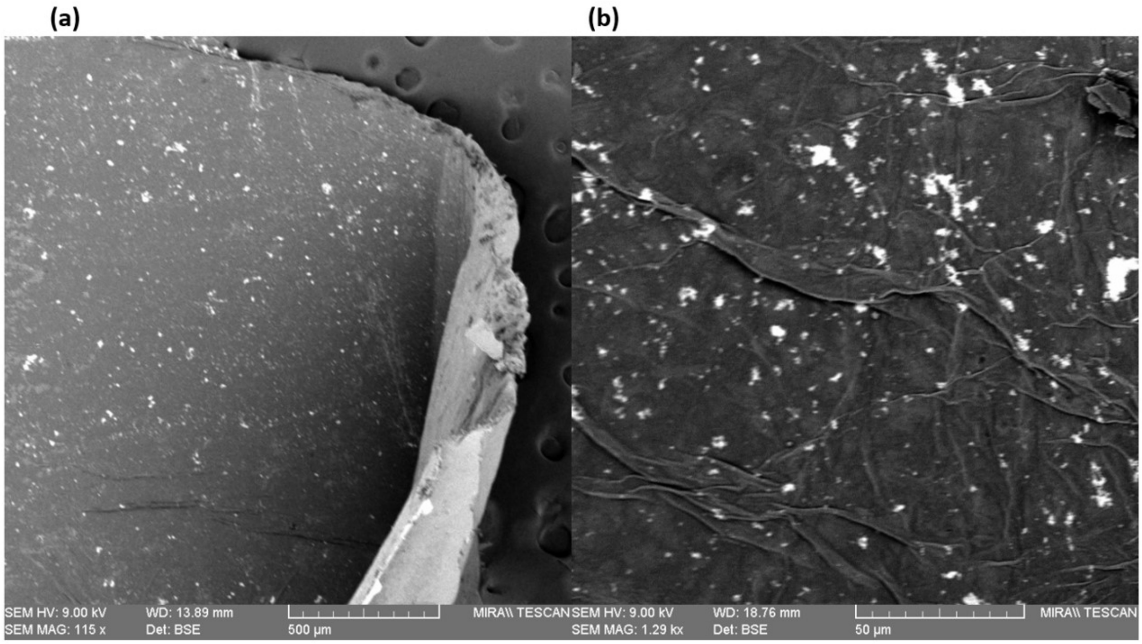

Figure 7. SEM micrographs of BC/TSNP films, showing distribution of TSNP clusters (white spots) at (**a**) 115× magnification and (**b**) 1.29 kx magnification.

3.3.2. Antimicrobial Activity of BC Blends

The antimicrobial evaluation of the prepared BC blends was performed by incubating the samples in inoculated broth, with *E. coli* and *S. aureus* as respective representatives of Gram-negative and Gram-positive strains. The results for PCL, PLA, and PHB blends incorporated with TSNPs can be observed in Figure 8. As it can be observed, the PCL and PLA blends showed no significant antimicrobial activity against either of the tested strains, even with the incorporation of TSNPs. Contrary to the results exhibited by the PLA and PCL blends, the blend made with PHB showed significant antimicrobial activity against both, *E. coli* and *S. aureus* strains after the incorporation of TSNPs. This is likely due to the highly homogeneous absorption of TSNPs that was observed in the BC/PHB blends, allowing for a visibly higher antimicrobial response compared to the other blends, which absorbed a smaller amount of TSNPs.

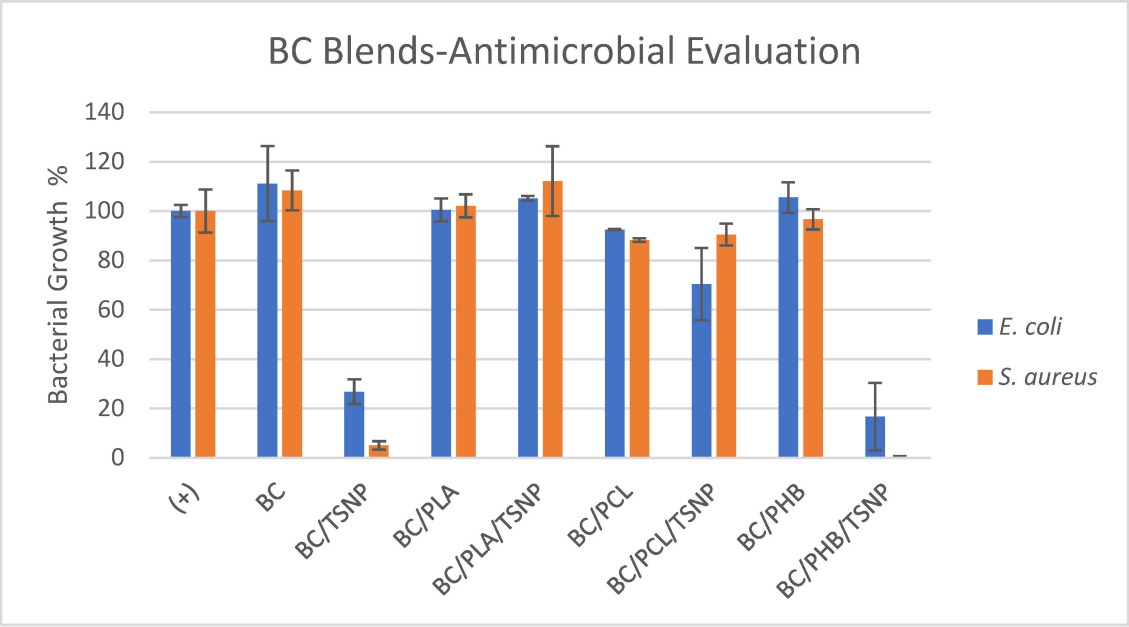

Figure 8. Results of antimicrobial evaluations for blends of BC with PLA, PCL, and PHB, incorporated with TSNPs, as well as bare materials used as control.

3.4. Evaluation of TSNP Application in Biosensing and Diagnostics

3.4.1. TSNP Gold Coating and Protection Check

The adapted method by Zhang et al. (2014) [38] was used in this study for coating of the TSNP, and the efficacy of the gold layer protection was evaluated with NaCl. Results show a TSNP $LSPR_{\lambda max}$ recorded at 579 nm, and after gold coating, the LSPR showed a red shift measured at 599 nm (Figure 9). Upon exposure to NaCl 20 mM, no blue shift in the LSPR peak was observed.

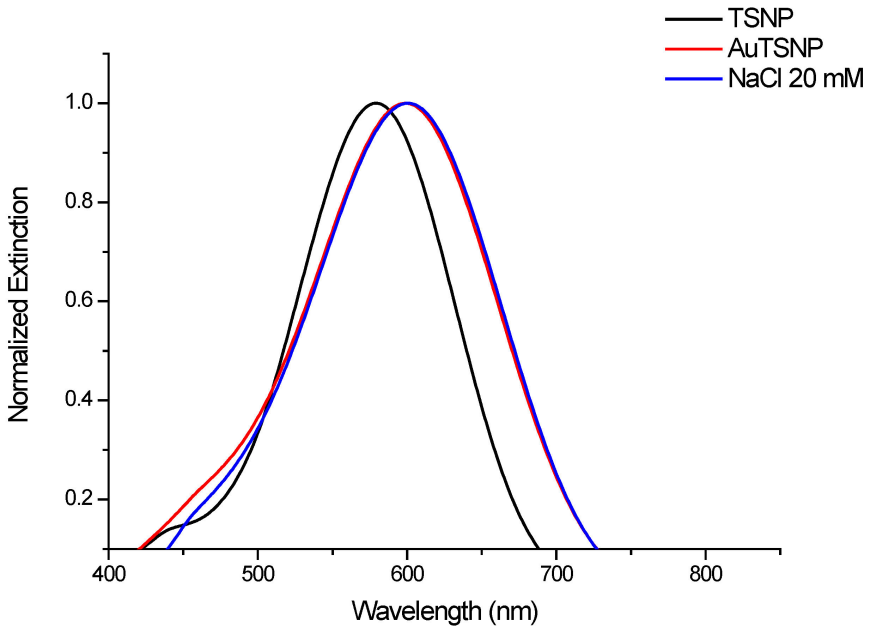

Figure 9. UV-Vis spectrum of TSNPs, AuTSNPs, and AuTSNPs exposed to NaCl 20 nM (protection check).

3.4.2. Sensitivity Test

The sensitivity test changes the refractive index of the medium in which the AuTSNPs are suspended, and can provide a measure of the nanoplates sensitivity without interfering with their stability. AuTSNP solution was added to increasing concentrations of sucrose solutions to evaluate the potential of the nanoplates for their use in sensing applications when there is a variation in the nanoplates' surrounding medium. Results (Figure 10) are in agreement with the reported outcomes by Charles et al., where the $LSPR_{\lambda max}$ of the spectra increases linearly as the sucrose concentration increases [54,56].

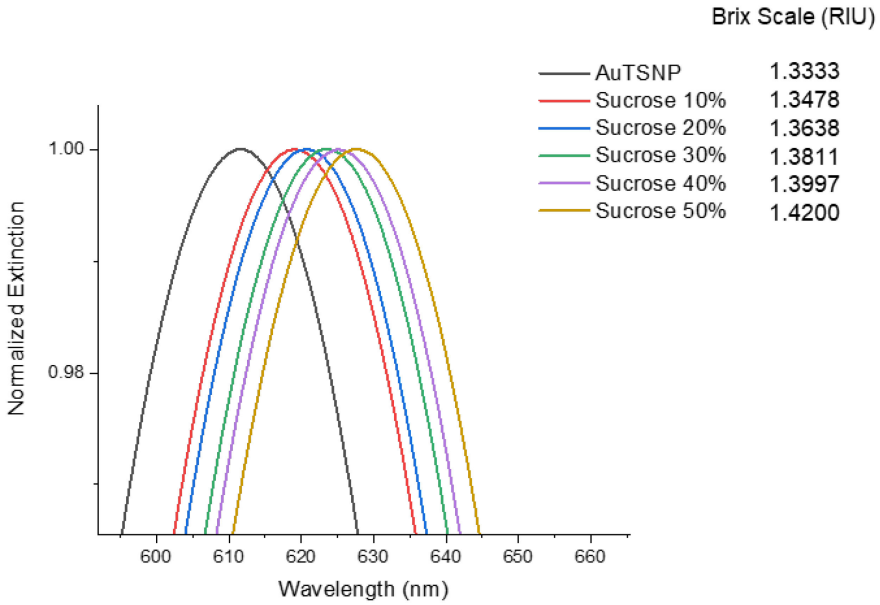

Figure 10. UV-Vis spectra of AuTSNPs suspended in a range of water–sucrose solutions.

3.4.3. Functionalization of FnPEGAuTSNPs and pH Monitoring

Prior to pH adjustment assays, AuTSNPs were coated with polyethylene glycol (PEGAuTSNP) to minimize contact between the Fn and the nanoplates' surface to avoid potential impact in the protein conformational behavior. Conformational changes in the protein were monitored by suspending the Fn-PEGAuTSNP in two phosphate buffers at pH 7.2 and pH 4.1, respectively. In Figure 11, the $LSPR_{\lambda max}$ of Fn-PEGAuTSNPs at pH 7 was measured at 633 nm; upon pH adjustment from pH 7 to pH 4, the $LSPR_{\lambda max}$ was measured to be 643 nm.

3.4.4. Determination of Adequate Fn Concentration

Several concentrations of Fn were added to aliquots of PEGAuTSNPs to determine the minimum amount of the protein to successfully cover the nanoplates and observe differences in the spectrum. One µg of anti-Fn was added afterwards to analyze binding. As reflected in Figure 12, changes in the spectra were observed with low concentrations of Fn. Results show that when higher concentrations of the protein were added to PEGAuTSNPs, longer red shifts were recorded as expected (Figure 12a). For all added concentrations of Fn, a red shift in the λ_{max} was observed upon addition of anti-Fn antibody (Figure 12b). In Figure 12c, expanded results show that shorter red shifts are recorded in higher Fn concentration samples once the anti-Fn antibody is added. This could be attributed to the anti-Fn binding to the excess of free unattached Fn within the nanoplate solution.

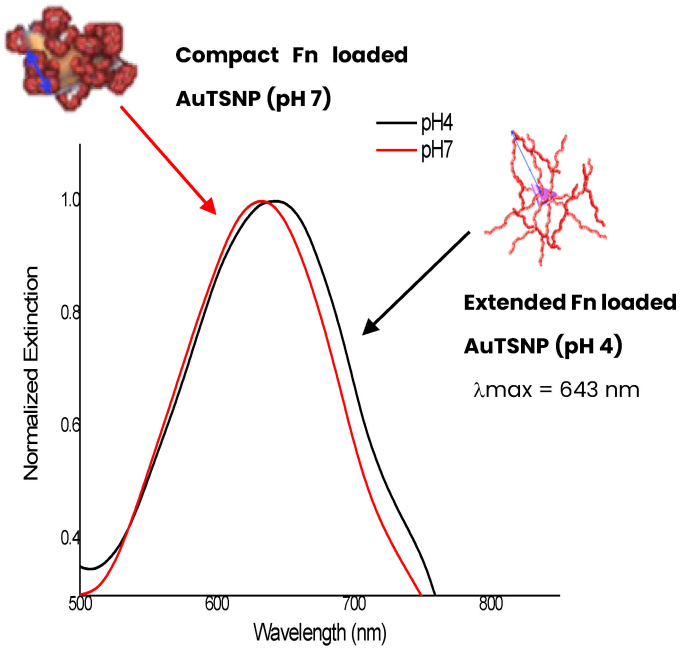

Figure 11. LSPR spectra of Fn-PEGAuTSNPs upon pH adjustment.

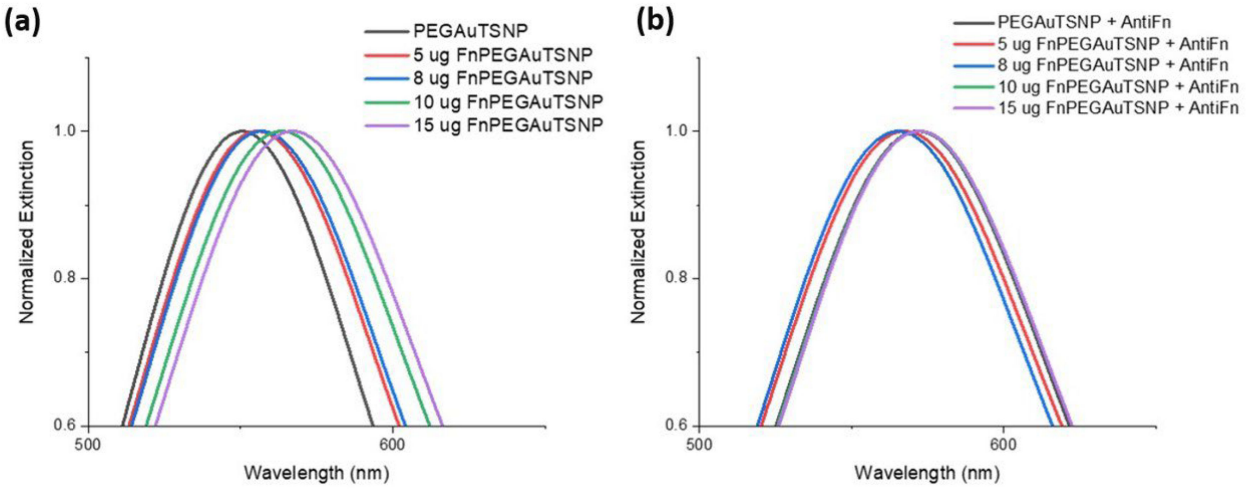

(c)

Fn Concentration	5µg	8 µg	10 µg	15 µg
$\Delta\lambda$	11	8	8	5

Figure 12. LSPR spectra of FnPEGAuTSNP samples (**a**) before and (**b**) after addition of anti-Fn antibody with (**c**) shift differences in λmax upon addition of anti-Fn.

3.4.5. Determination of Adequate Anti-Fn Antibody Concentration

The limit of detection of the Ag-Ab system was determined by exposing a sample of Fn-PEGAuTSNPs to increasing concentrations of anti-Fn antibody. As observed in Figure 11b, there is evident red shifting as the concentration of anti-Fn increases, which indicates intensifying binding of the antibody to the Fn functionalized nanoplates. There is detection of Fn-anti-Fn binding with antibody concentrations as low as 0.01 mg/mL, and shorter redshifts are recorded for the highest concentrations of antibody, indicating system saturation from 0.212 mg/mL of the anti-Fn antibody (Figure 13a).

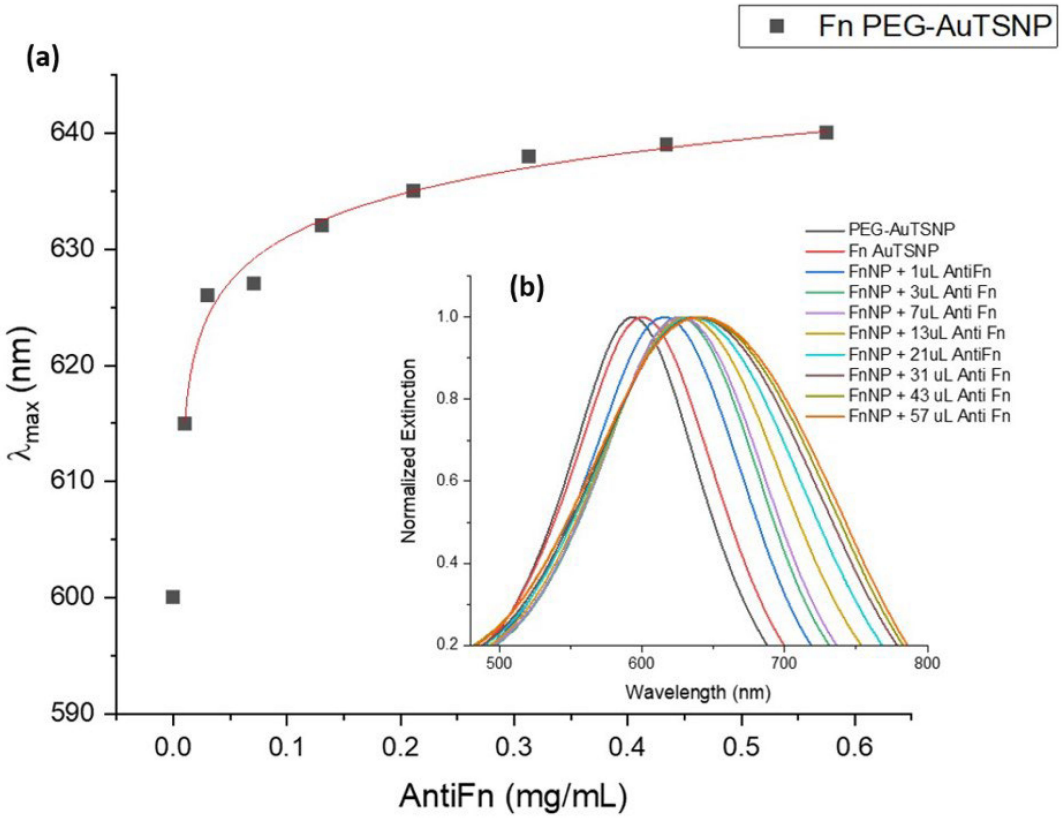

Figure 13. (**a**) LSPR peak shift as a function of anti-Fn antibody concentration for Fn-PEGAuTSNPs (**b**) LSPR spectra of Fn-PEGAuTSNPs upon addition of increasing concentrations of anti-Fn.

4. Discussion

It was established that different morphologies of AgNPs present different properties to one another. They can be synthesized in a range of shapes, including spheres, rods, wires, triangles, and cubes, each possessing unique characteristics. Spheres possess excellent stability and dispersibility, while in the case of TSNPs and other nanostructures with sharp geometries, it was observed that the tips can provide a greater electric field enhancement, allowing optical properties to be more easily tuned and controlled [17]. Furthermore, the same sharp edges and corners present in TSNPs make them more susceptible to oxidation, resulting in a higher rate of Ag+ ions released compared to spherical NPs, resulting in a higher antimicrobial activity [16]. In the solution form, color variations provide a visual means to differentiate and identify the specific shapes of silver nanoparticles: spheres are exhibiting yellow color while in the form of triangles the solution acquires a distinct blue (Figure 1).

In the original protocol of [50] the concentration of silver is 16.692 ppm in the TSNP solution, where results show broad localized surface plasmon resonances (LSPR) of more than 130 nm full width at half maximum (FWHM) (Figure 2). The broad FWHM of the TSNP spectrum can be attributed to the inhomogeneity of sizes and nanoparticle shapes in the solution. This can reduce the nanoplate sensitivity, which is a critical property in TSNPs when used in nanosensing applications [56]. The triangular morphology of the TSNP prepared through this method was evaluated using TEM on a previous study performed by our team (Figure 3), where the same synthesis method for the TSNP was used [55]. The TEM images, the color, and the spectra readings of our TSNP solution come in accordance to other studies that used similar seed-mediated methods to synthesize TSNPs [5,50,54]. An increase in the produced volume and in the amount of silver in the nanoplate solution was achieved, and the resulting LSPR spectrum demonstrated that a reduced water amount does not have an impact on the LSPR behavior of the TSNP (Figures 4 and 5). It was

reported that high sensitivity of the TSNP LSPR is due to the high proportion of triangular geometries and the platelet structure of the nanoparticles. Furthermore, compared to single silver nanoparticles, the sensitivity is increased in highly organized silver nanoparticle aggregates (in solution) [56].

Silver nanoplates emerged as a remarkable tool in the development of antimicrobial materials, offering unique properties that make it a valuable asset in the fight against microbial infections. Through the incorporation of silver into diverse materials, such as coatings, textiles, and medical devices, significant advancements were made in the field of antibacterial therapeutics [57]. Taking into consideration previously mentioned properties and the lack of research on TSNPs for antimicrobial applications in polymeric materials, studies were performed to evaluate their suitability as antimicrobial agents for polymers and biopolymers. The TSNP synthesis method used in this study resulted in a highly concentrated TSNP solution, which is desirable in order to include the TSNPs into polymer processing. Using this method, the amount of water required to be removed was decreased, while the number of nanoplates available for the process was increased. Incorporation of TSNPs in biopolymer blends with a lower percentage of incorporated polymer (PHB) resulted in higher absorption of the aqueous TSNP solution by the hydrophilic BC matrix compared to the PLA and PCL blends that incorporated a higher percentage of polymer on the BC. Previous studies also evaluated the integration of TSNPs into BC supplemented with curcumin [53], as well as their integration into pure PCL and PLA using a solvent casting method, resulting in improved properties of BC and biocompatible materials [55]. BC/PHB blends with TSNPs (Figure 6a) showed significant decrease in microbial growth for both tested bacterial strains; this is attributed to the higher amount of absorbed TSNPs compared to the PCL and PLA blends (Figure 8). These results come in accordance with previous work on the incorporation of AgNPs into polymeric materials, where a higher antimicrobial response is exhibited on the materials that are able to maintain a higher rate of silver and Ag+ ions release [58]. Contrary to the previously reported study for evaluation of the antimicrobial activity of TSNPs incorporated into polymeric materials through solvent casting [55], the BC/PHB blend exhibited a higher antimicrobial response towards the Gram-negative strain under the examined conditions.

Proteins are known to easily bind to gold and silver nanoparticles spontaneously. It occurs through ionic or hydrophobic interactions [59]. Nanoparticles may be pre-functionalized with specific proteins, which will determine which new protein will attach to the newly formed NP-protein system [60]. According to Aherne et al., line widths of the LSPR are reduced as the nanoplate volume increases, which improves sensitivity of the nanoplates. Furthermore, a blue shift in the LSPR can be observed (from 600 to 530 nm) upon silver seed volume adjustment, resulting in a size reduction of the nanoplates [50]. This can be advantageous for the use of TSNPs in biosensing, since it allows for a higher range in which shifts in the spectrum can be easily detected within the UV-Vis range (Figures 4 and 5). Unprotected TSNPs can be highly susceptible to degradation or etching by catalytic oxidation in the presence of chlorine or other reactive ions. This can lead to alterations of the geometry and structure of the TSNP, normally resulting in a substantial blue shift in their spectrum and impairing their LSPR properties [38]. Different coatings can be used to protect the TSNP structure; nonetheless, most coatings will also affect the plasmonic response of the nanoparticles. A method used by [38] proved to successfully coat TSNP edges with a layer of gold, providing the nanoparticles with protection from etching while allowing them to maintain their plasmonic response and refractive index sensitivity. Results of this study are in accordance to the results reported by the [38] deposition of a thin layer of gold in the triangular nanoplate edges at low Ag:Au ratios, successfully protecting the nanoplates without causing any structural damages associated with galvanic replacement (Figure 9). Moreover, no major changes in the nanoplates' optical properties occurred besides an enhancement of its optical sensitivity. The LSPR spectrum at pH 4 was redshifted by 10 nm upon Fn extension due to a higher refractive index surrounding the nanoplates. The presence of the compact protein strand on top of the nanoparticle

surface occupies a larger surface area; however, it does not bulge from the surface more than an elongated Fn strand, which can explain the shift in the spectrum. As presented in Figure 10, sucrose sensitivity assay confirmed that $LSPR_{\lambda max}$ of the spectra directly correlates to sucrose concentration [54,56]. In order to minimize any potential impact on the protein's conformational behavior, AuTSNPs were coated with PEG in order to avoid any direct interaction between the nanoplates' surface and the protein, thus reducing the likelihood of any influence on its conformation. Conformational changes of the protein were monitored by suspending the Fn-PEGAuTSNP in two phosphate buffers at pH 7.2 and pH 4.1 since Fn is known to change its structure upon pH variations (Figure 11). Fn has an uncoiled conformation when in acidic or high salt conditions, whereas within low salt conditions it shows a "coiled compact" conformation [61]. In previous studies where Fn conformational changes are analyzed within different pH environments, Fn is reported to have a hydrodynamic radius of 23 nm when compacted, and when it extends the radius increases up to 130 nm for single Fn strands [43,44]. Fn can form much larger strands as networks and fibrils can develop and be mediated within the extracellular matrix (ECM) [62].

When it comes to determination of adequate concentration of Fn, as reflected in Figure 12, changes in the spectra were observed with low concentrations of Fn. On the other hand, Fn-anti-Fn binding with antibody concentrations as low as 0.01 mg/mL were detected, and shorter redshifts are recorded for the highest concentrations of antibody, indicating system saturation from 0.212 mg/mL of the anti-Fn antibody (Figure 13). This correlates with the studies by Zhang et al. (2014) where cytidine 50-diphosphocholine (PC)-coated AuTSNPs detect C-reactive protein (CRP) in concentrations as low as 0.0033 mg/L, showing the remarkable features of the AuTSNPs and their wide-ranging limits of detection [38]. Detection limits for several other nanobiosensors were reported with ranging limits between 0.8 and 40 ng/mL for gold nanoparticles and 12 pM for Cu nanoclusters, among others [63].

This demonstrates the ability of AuTSNPs for their use as versatile and efficient platforms for immunnoassays, opening up exciting possibilities for cutting-edge diagnostic applications. Functionalization of these AuTSNPs with specific antibodies or antigens could facilitate the detection and quantification of analytes. The integration of AuTSNPs into immunoassay platforms has the potential to transform disease diagnosis and biomedical research, providing a powerful tool for rapid detection of diseases with high sensitivity.

5. Conclusions

In conclusion, different morphologies of silver nanoparticles exhibit unique properties. Spherical AgNPs are stable and dispersible, while triangular silver nanoplates with sharp edges enhanced electric field enhancement and antimicrobial activity. The synthesis method used in this study resulted in a highly concentrated TSNP solution, which is desirable for incorporating TSNPs into polymer processing. TSNPs incorporated into biopolymer blends, particularly BC/PHB blends, showed significant antimicrobial activity against bacterial strains compared to blends with other polymers such as PCL and PLA. The higher absorption of TSNPs by the hydrophilic BC matrix contributed to this antimicrobial response. Adjusting the silver seed volume reduces nanoplate size, improving sensitivity for biosensing applications. Coating the edges of TSNPs with a layer of gold protected the nanoparticles from degradation without impairing their plasmonic response and refractive index sensitivity. The functionalization of AuTSNPs with specific antibodies or antigens enables their use as versatile platforms for immunological assays, facilitating the rapid and sensitive detection of diseases. Future work will include investigation of the proposed detection system's selectivity fare in the presence of physiological elements.

Overall, the unique properties and versatility of silver nanoplates, particularly TSNPs, make them valuable assets in various fields, including antimicrobial materials, nanosensing, and biomedical research. Further exploration and utilization of these nanoparticles hold

great potential for advancements in antibacterial therapeutics, disease diagnosis, and biomedical applications.

Author Contributions: L.G.R.B. conceptualization, methodology, investigation, writing—original draft preparation; E.L.G. conceptualization, methodology, investigation, writing—original draft preparation; M.M. conceptualization, writing—original draft preparation, writing—review and editing, supervision; M.H. methodology, writing—original draft preparation, supervision; R.P. methodology, writing—original draft preparation, supervision; D.M.D. methodology, supervision; M.B.-F. conceptualization, methodology, supervision, and funding acquisition. All authors have read and agreed to the published version of the manuscript.

Funding: This research was supported by the Technological University of The Shannon through the President Seed Fund, the Government of Ireland International Education Scholarship 2018/2019, the European Union's Horizon 2020 Research and Innovation program [grant number: 870292 (BioICEP)]; European Union's Horizon Europe EIC Pathfinder program [grant number: 101046758 (EcoPlastiC)].

Institutional Review Board Statement: Not applicable.

Informed Consent Statement: Not applicable.

Data Availability Statement: https://zenodo.org/ (accessed on 5 May 2023).

Conflicts of Interest: The authors declare no conflict of interest.

References

1. Tanasa, E.; Zaharia, C.; Radu, I.C.; Surdu, V.A.; Vasile, B.S.; Damian, C.M.; Andronescu, E. Novel Nanocomposites Based on Functionalized Magnetic Nanoparticles and Polyacrylamide: Preparation and Complex Characterization. *Nanomaterials* **2019**, *9*, 1384. [CrossRef]
2. Andronescu, E.; Predoi, D.; Neacsu, I.A.; Paduraru, A.V.; Musuc, A.M.; Trusca, R.; Oprea, O.; Tanasa, E.; Vasile, O.R.; Nicoara, A.I.; et al. Photoluminescent Hydroxylapatite: Eu^{3+} Doping Effect on Biological Behaviour. *Nanomaterials* **2019**, *9*, 1187. [CrossRef] [PubMed]
3. Lee, K.W.; Kim, Y.H.; Du, W.X.; Kim, J.Y. Stretchable and Low-Haze Ag-Nanowire-Network 2-D Films Embedded into a Cross-Linked Polydimethylsiloxane Elastomer. *Nanomaterials* **2019**, *9*, 576. [CrossRef]
4. Jeevanandam, J.; Barhoum, A.; Chan, Y.S.; Dufresne, A.; Danquah, M.K. Review on Nanoparticles and Nanostructured Materials: History, Sources, Toxicity and Regulations. *Beilstein J. Nanotechnol.* **2018**, *9*, 1050–1074. [CrossRef] [PubMed]
5. Kelly, J.M.; Keegan, G.; Brennan-Fournet, M.E. Triangular Silver Nanoparticles: Their Preparation, Functionalisation and Properties. *Acta Phys. Pol. A* **2012**, *122*, 337–345. [CrossRef]
6. Zhang, C.; Huang, Q.; Cui, Q.; Ji, C.; Zhang, Z.; Chen, X.; George, T.; Zhao, S.; Guo, L.J. High-Performance Large-Scale Flexible Optoelectronics Using Ultrathin Silver Films with Tunable Properties. *ACS Appl. Mater. Interfaces* **2019**, *11*, 27216–27225. [CrossRef]
7. Bhardwaj, A.K.; Sundaram, S.; Yadav, K.K.; Srivastav, A.L. An Overview of Silver Nano-Particles as Promising Materials for Water Disinfection. *Environ. Technol. Innov.* **2021**, *23*, 101721. [CrossRef]
8. Takáč, P.; Michalková, R.; Čižmáriková, M.; Bedlovičová, Z.; Balážová, Ľ.; Takáčová, G. The Role of Silver Nanoparticles in the Diagnosis and Treatment of Cancer: Are There Any Perspectives for the Future? *Life* **2023**, *13*, 466. [CrossRef]
9. Gomes, H.I.O.; Martins, C.S.M.; Prior, J.A.V. Silver Nanoparticles as Carriers of Anticancer Drugs for Efficient Target Treatment of Cancer Cells. *Nanomaterials* **2021**, *11*, 964. [CrossRef]
10. Shanmuganathan, R.; Karuppusamy, I.; Saravanan, M.; Muthukumar, H.; Ponnuchamy, K.; Ramkumar, V.S.; Pugazhendhi, A. Synthesis of Silver Nanoparticles and Their Biomedical Applications—A Comprehensive Review. *Curr. Pharm. Des.* **2019**, *25*, 2650–2660. [CrossRef]
11. Gopinath, P.; Gogoi, S.K.; Chattopadhyay, A.; Ghosh, S.S. Implications of Silver Nanoparticle Induced Cell Apoptosis for in Vitro Gene Therapy. *Nanotechnology* **2008**, *19*, 075104. [CrossRef]
12. Suter, S.; Haussener, S. Optimizing Mesostructured Silver Catalysts for Selective Carbon Dioxide Conversion into Fuels. *Energy Environ. Sci.* **2019**, *12*, 1668–1678. [CrossRef]
13. Lee, S.H.; Jun, B.H. Silver Nanoparticles: Synthesis and Application for Nanomedicine. *Int. J. Mol. Sci.* **2019**, *20*, 865. [CrossRef]
14. Güzel, R.; Erdal, G. *Synthesis of Silver Nanoparticles*; IntechOpen: London, UK, 2016; Chapter 1; Volume 13. [CrossRef]
15. Le, V.T.; Bach, L.G.; Pham, T.T.; Le, N.T.T.; Ngoc, U.T.P.; Tran, D.H.N.; Nguyen, D.H. Synthesis and Antifungal Activity of Chitosan-Silver Nanocomposite Synergize Fungicide against Phytophthora Capsici. *J. Macromol. Sci. Part A Pure Appl. Chem.* **2019**, *56*, 522–528. [CrossRef]
16. Lu, W.; Yao, K.; Wang, J.; Yuan, J. Ionic Liquids-Water Interfacial Preparation of Triangular Ag Nanoplates and Their Shape-Dependent Antibacterial Activity. *J. Colloid Interface Sci.* **2015**, *437*, 35–41. [CrossRef]

17. Kelly, K.L.; Coronado, E.; Zhao, L.L.; Shatz, G.C. The Optical Properties of Metal Nanoparticles_The Influence of Size, Shape, and Dielectric Environment. *J. Phys. Chem. B* **2003**, *107*, 668–677. [CrossRef]
18. Pastoriza-Santos, I.; Liz-Marzán, L.M. Colloidal Silver Nanoplates. State of the Art and Future Challenges. *J. Mater. Chem.* **2008**, *18*, 1724–1737. [CrossRef]
19. Qing, Y.; Cheng, L.; Li, R.; Liu, G.; Zhang, Y.; Tang, X.; Wang, J.; Liu, H.; Qin, Y. Potential Antibacterial Mechanism of Silver Nanoparticles and the Optimization of Orthopedic Implants by Advanced Modification Technologies. *Int. J. Nanomed.* **2018**, *13*, 3311–3327. [CrossRef]
20. Siritongsuk, P.; Hongsing, N.; Thammawithan, S.; Daduang, S.; Klaynongsruang, S.; Tuanyok, A.; Patramanon, R. Two-Phase Bactericidal Mechanism of Silver Nanoparticles against Burkholderia Pseudomallei. *PLoS ONE* **2016**, *11*, e0168098. [CrossRef]
21. Pal, S.; Tak, Y.K.; Song, J.M. Does the Antibacterial Activity of Silver Nanoparticles Depend on the Shape of the Nanoparticle? A Study of the Gram-Negative Bacterium Escherichia Coli. *Appl. Environ. Microbiol.* **2007**, *73*, 1712–1720. [CrossRef]
22. Abbas, M.; Naeem, N.; Iftikhar, H.; Latif, U. *Synthesis, Characterization and Antimicrobial Properties of Silver Nanocomposites*; IntechOpen: London, UK, 2018; Volume i, Chapter 4; p. 13. [CrossRef]
23. Knauer, A.; Csáki, A.; Fritzsche, W.; Serra, C.A.; Leclerc, N.; Michael Köhler, J. Micro Continuous Flow-through Synthesis of Triangular Silver Nanoprisms and Their Incorporation in Complexly Composed Polymer Microparticles. *Chem. Eng. J.* **2013**, *227*, 191–197. [CrossRef]
24. Audoit, J.; Laffont-dantras, L.; Lonjon, A.; Dantras, E.; Audoit, J.; Laffont-dantras, L.; Lonjon, A.; Dantras, E.; Percolative, C.L. Percolative Silver Nanoplates/PVDF Nanocomposites: Bulk and Surface Electrical Conduction. *Polymer* **2016**, *78*, 104–110. [CrossRef]
25. Zhang, J.; Sun, Y.; Zhang, H.; Xu, B.; Zhang, H.; Song, D. Preparation and Application of Triangular Silver Nanoplates/Chitosan Composite in Surface Plasmon Resonance Biosensing. *Anal. Chim. Acta* **2013**, *769*, 114–120. [CrossRef] [PubMed]
26. Reynoso-García, P.J.; Güizado-Rodríguez, M.; Barba, V.; Ramos-Ortiz, G.; Martínez-Gutiérrez, H. Stabilization of Silver Nanoparticles with a Dithiocarbamate Ligand and Formation of Nanocomposites by Combination with Polythiophene Derivative Nanoparticles. *Adv. Condens. Matter Phys.* **2018**, *2018*, 4376051. [CrossRef]
27. Kudryashov, M.; Logunov, A.; Gogova, D.; Mashin, A.; De Filpo, G. Ag/PVP/PAN Nanocomposites with Triangular Nanoprisms of Silver Synthesized by UV-Induced Polymerization: Morphology Manipulation and Optical Properties Tuning. *Opt. Mater.* **2020**, *101*, 109746. [CrossRef]
28. Djafari, J.; Fernández-Lodeiro, C.; Fernández-Lodeiro, A.; Silva, V.; Poeta, P.; Igrejas, G.; Lodeiro, C.; Capelo, J.L.; Fernández-Lodeiro, J. Exploring the Control in Antibacterial Activity of Silver Triangular Nanoplates by Surface Coating Modulation. *Front. Chem.* **2019**, *6*, 677. [CrossRef]
29. Vo, Q.K.; Phung, D.D.; Nguyen, Q.N.V.; Thi, H.H.; Thi, N.H.N.; Thi, P.P.N.; Bach, L.G.; Tan, L. Van Controlled Synthesis of Triangular Silver Nanoplates by Gelatin-Chitosan Mixture and the Influence of Their Shape on Antibacterial Activity. *Processes* **2019**, *7*, 873. [CrossRef]
30. Velgosova, O.; Mačák, L.; Lisnichuk, M.; Vojtko, M. Synthesis and Analysis of Polymorphic Silver Nanoparticles and Their Incorporation into the Polymer Matrix. *Polymers* **2022**, *14*, 2666. [CrossRef]
31. Unser, S.; Bruzas, I.; He, J.; Sagle, L. Localized Surface Plasmon Resonance Biosensing: Current Challenges and Approaches. *Sensors* **2015**, *15*, 15684–15716. [CrossRef]
32. Mauriz, E.; Dey, P.; Lechuga, L.M. Advances in Nanoplasmonic Biosensors for Clinical Applications. *Analyst* **2019**, *144*, 7105–7129. [CrossRef]
33. Tang, Y.; Zeng, X.; Liang, J. Surface Plasmon Resonance: An Introduction to a Surface Spectroscopy Technique. *J. Chem. Educ.* **2010**, *87*, 742–746. [CrossRef]
34. Aherne, D.; Charles, D.E.; Brennan-Fournet, M.E.; Kelly, J.M.; Gun'ko, Y.K. Etching-Resistant Silver Nanoprisms by Epitaxial Deposition of a Protecting Layer of Gold at the Edges. *Langmuir* **2009**, *25*, 10165–10173. [CrossRef]
35. Willets, K.A.; Van Duyne, R.P. Localized Surface Plasmon Resonance Spectroscopy and Sensing. *Annu. Rev. Phys. Chem.* **2007**, *58*, 267–297. [CrossRef]
36. Petryayeva, E.; Krull, U.J. Localized Surface Plasmon Resonance: Nanostructures, Bioassays and Biosensing—A Review. *Anal. Chim. Acta* **2011**, *706*, 8–24. [CrossRef]
37. Loiseau, A.; Asila, V.; Boitel-Aullen, G.; Lam, M.; Salmain, M.; Boujday, S. Silver-Based Plasmonic Nanoparticles for and Their Use in Biosensing. *Biosensors* **2019**, *9*, 78. [CrossRef]
38. Zhang, Y.; Charles, D.E.; Ledwith, D.M.; Aherne, D.; Cunningham, S.; Voisin, M.; Blau, W.J.; Gun'Ko, Y.K.; Kelly, J.M.; Brennan-Fournet, M.E. Wash-Free Highly Sensitive Detection of C-Reactive Protein Using Gold Derivatised Triangular Silver Nanoplates. *RSC Adv.* **2014**, *4*, 29022–29031. [CrossRef]
39. Michael Kotlarchyk Scattering Theory. In *Encyclopedia of Spectroscopy and Spectrometry*; Academic Press: Cambridge, MA, USA, 1999; pp. 2074–2084.
40. Wu, C.; Zhou, X.; Wei, J. Localized Surface Plasmon Resonance of Silver Nanotriangles Synthesized by a Versatile Solution Reaction. *Nanoscale Res. Lett.* **2015**, *10*, 354. [CrossRef]
41. Zhang, C.; Qiu, M.; Wang, J.; Liu, Y. Recent Advances in Nanoparticle-Based Optical Sensors for Detection of Pesticide Residues in Soil. *Biosensors* **2023**, *13*, 415. [CrossRef]

42. Liu, L.; Liang, X.; Qiu, G.; Guo, C.; Chan, Y.K.; Wu, C.-M.L. Self-Assembly Silver Nanoparticles Decorated on Gold Nanoislands for Label-Free Localized Surface Plasmon Resonance Biosensing. *Adv. Mater. Interfaces* **2022**, *9*, 2200339. [CrossRef]
43. Brennan-Fournet, M.E.; Huerta, M.; Zhang, Y.; Malliaras, G.; Owens, R.M. Detection of Fibronectin Conformational Changes in the Extracellular Matrix of Live Cells Using Plasmonic Nanoplates. *J. Mater. Chem. B* **2015**, *3*, 9140–9147. [CrossRef]
44. Rodriguez Barroso, L.G.; Azaman, F.A.; Pogue, R.; Devine, D.; Fournet, M.B. Monitoring In Vitro Extracellular Matrix Protein Conformations in the Presence of Biomimetic Bone-Regeneration Scaffolds Using Functionalized Gold-Edge-Coated Triangular Silver Nanoparticles. *Nanomaterials* **2023**, *13*, 57. [CrossRef] [PubMed]
45. Vinayagam, S.; Rajaiah, P.; Mukherjee, A.; Natarajan, C. DNA-Triangular Silver Nanoparticles Nanoprobe for the Detection of Dengue Virus Distinguishing Serotype. *Spectrochim. Acta Part A Mol. Biomol. Spectrosc.* **2018**, *202*, 346–351. [CrossRef] [PubMed]
46. Cai, T.; Gao, Y.; Yan, J.; Wu, Y.; Di, J. Visual Detection of Glucose Using Triangular Silver Nanoplates and Gold Nanoparticles. *RSC Adv.* **2017**, *7*, 29122–29128. [CrossRef]
47. Fang, X.; Ren, H.; Zhao, H.; Li, Z. Ultrasensitive Visual and Colorimetric Determination of Dopamine Based on the Prevention of Etching of Silver Nanoprisms by Chloride. *Microchim. Acta* **2017**, *184*, 415–421. [CrossRef]
48. Li, L.; Zhang, L.; Zhao, Y.; Chen, Z. Colorimetric Detection of Hg(II) by Measurement the Color Alterations from the "before" and "after" RGB Images of Etched Triangular Silver Nanoplates. *Microchim. Acta* **2018**, *185*, 235. [CrossRef]
49. Furletov, A.A.; Apyari, V.V.; Garshev, A.V.; Dmitrienko, S.G.; Zolotov, Y.A. Triangular Silver Nanoplates as a Spectrophotometric Reagent for the Determination of Mercury(II). *J. Anal. Chem.* **2017**, *72*, 1203–1207. [CrossRef]
50. Aherne, D.; Ledwith, D.M.; Gara, M.; Kelly, J.M. Optical Properties and Growth Aspects of Silver Nanoprisms Produced by a Highly Reproducible and Rapid Synthesis at Room Temperature. *Adv. Funct. Mater.* **2008**, *18*, 2005–2016. [CrossRef]
51. Solomon, S.D.; Bahadory, M.; Jeyarajasingam, A.V.; Rutkowsky, S.A.; Boritz, C.; Mulfinger, L. Synthesis and Study of Silver Nanoparticles. *J. Chem. Educ.* **2007**, *84*, 322–325.
52. Etacheri, V.; Georgekutty, R.; Seery, M.K.; Pillai, S.C. Single Step Morphology-Controlled Synthesis of Silver Nanoparticles. *Mater. Res. Soc. Symp. Proc.* **2010**, *1217*, 7–13. [CrossRef]
53. Garcia, E.L.; Mojicevic, M.; Milivojevic, D.; Aleksic, I.; Vojnovic, S.; Stevanovic, M.; Murray, J.; Attallah, O.A.; Devine, D.; Fournet, M.B. Enhanced Antimicrobial Activity of Biocompatible Bacterial Cellulose Films via Dual Synergistic Action of Curcumin and Triangular Silver Nanoplates. *Int. J. Mol. Sci.* **2022**, *23*, 12198. [CrossRef]
54. Charles, D.E.; Aherne, D.; Gara, M.; Ledwith, D.M.; Gun, Y.K.; Kelly, J.M.; Blau, W.J.; Brennan-fournet, M.E. Versatile Solution Phase Triangular Silver Nanoplates for Highly Sensitive Plasmon Resonance Sensing. *ACS Nano* **2010**, *4*, 55–64. [CrossRef] [PubMed]
55. Garcia, E.L.; Attallah, O.A.; Mojicevic, M.; Devine, D.M.; Fournet, M.B. Antimicrobial Active Bioplastics Using Triangular Silver Nanoplate Integrated Polycaprolactone and Polylactic Acid Films. *Materials* **2021**, *14*, 1132. [CrossRef] [PubMed]
56. Charles, D.; Fournet, P.; Cunningham, S.; Ledwith, D.; Kelly, J.M.; Blau, W.; Fournet, M.B. A Sensitivity Study of the Localised Surface Plasmon Resonance of High-Definition Structured Silver Nanoparticles in Solution. *Plasmon. Met. Nanostruct. Their Opt. Prop. VI* **2008**, *7032*, 70322G. [CrossRef]
57. Bruna, T.; Maldonado-Bravo, F.; Jara, P.; Caro, N. Silver Nanoparticles and Their Antibacterial Applications. *Int. J. Mol. Sci.* **2021**, *22*, 7202. [CrossRef]
58. Lyutakov, O.; Goncharova, I.; Rimpelova, S.; Kolarova, K.; Svanda, J.; Svorcik, V. Silver Release and Antimicrobial Properties of PMMA Films Doped with Silver Ions, Nano-Particles and Complexes. *Mater. Sci. Eng. C* **2015**, *49*, 534–540. [CrossRef] [PubMed]
59. Szymanski, M.S.; Porter, R.A. Preparation and Quality Control of Silver Nanoparticle-Antibody Conjugate for Use in Electrochemical Immunoassays. *J. Immunol. Methods* **2013**, *387*, 262–269. [CrossRef]
60. Saptarshi, S.R.; Duschl, A.; Lopata, A.L. Interaction of Nanoparticles with Proteins: Relation to Bio-Reactivity of the Nanoparticle. *J. Nanobiotechnol.* **2013**, *11*, 26. [CrossRef]
61. Maurer, L.M.; Ma, W.; Mosher, D.F. Dynamic Structure of Plasma Fibronectin. *Crit. Rev. Biochem. Mol. Biol.* **2016**, *51*, 213–227. [CrossRef]
62. Tooney, N.M.; Mosesson, M.W.; Amrani, D.L.; Hainfeld, J.F.; Wall, J.S. Solution and Surface Effects on Plasma Fibronectin Structure. *J. Cell Biol.* **1983**, *97*, 1686–1692. [CrossRef]
63. Karabulut, G.; Üllen, N.B.; Karakuş, S. Nanostructures in Biosensors Development and Applications. In *Biosignal Processing*; IntechOpen: London, UK, 2022; ISBN 978-1-80355-562-1.